DYNAMIC THERMAL ANALYSIS FOR LUNAR SURFACE OPERATIONS: CURRENT STATUS OF THE THERMOS APPROACH

P. Hager, R. Haber, D. Kraus, S. Nogina, A. Sievers, T. Tattusch, U. Walter
Technische Universität München, Institute of Astronautics, Boltzmannstraße 15, 85748 Garching b. München, Germany

Abstract

For surface-craft such as rovers, the lunar surface provides a challenging thermal environment. Environmental temperatures between 40 K and 400 K are encountered. Spatial temperature gradients of about 200 K within a few centimeters are possible. Heat transfer is dominated by radiation and no atmosphere dampens the incoming solar heat flux. Future lunar rovers will have to move through this demanding environment and are subject to varying heat loads. This scenario is the focus of the Thermal Moon Simulator (TherMoS) of which we present the current status in this paper.

Today's thermal designs for rovers to be used on the Moon are traditionally based on worst case scenarios. These minimum/maximum designs are either heavy or restricted to certain selenographical regions. Commercial thermal tools like ESATAN-TMS®, Thermal Desktop® or Thermica® are well suited to account for the thermal design questions arising for spacecraft in orbits and for static objects such as bases on the Moon. They are not suited to simulate the dynamic temperature behavior caused by rover movement and large environmental heat flux from multiple directions. The Institute of Astronautics at the Technische Universität München investigates the question in which cases and on which scales the dynamic behavior of thermal problems in space applications are necessary in contrast to the worst-case approach. Target groups for this tool are thermal engineers, systems engineers, and project managers. In this context the TherMoS – computer simulation tool is being developed.

The TherMoS tool is composed of a topographic module, a regolith module, a module for craters and boulders, a module for orbit propagation and lunar orientation, a ray tracing module, a geometry assembly module, a thermal solver module and a post-processing module. All but the ray tracing module are implemented in MATLAB® and the ray tracing algorithm uses NVIDIA OptiX®. The global topography is based on a publicly available dataset measured by the LALT (Laser ALTimeter) instrument onboard the Japanese probe Kaguya. The regolith model improves on older models by integrating temperature dependent values and a depth dependent regolith density profile. The orbit propagator is based on the VSOP2000A, a semi-analytical power-series approximation. The TherMoS simulation allows importing and manipulating geometric models from other software. The ray tracing algorithm determines the radiative heat transfer between the lunar surface and the surface craft. It takes into account the solar fluxes, the IR radiation and their diffusive reflections. The ray tracing functionality runs on a graphics processor and is called from MATLAB®. In MATLAB® the thermal calculations are performed; temperatures and temperature dependent material properties are recalculated. The orbit propagator alters the local Sun vector during the simulation. Manipulation of the geometry between calculation steps allows for the movement of the surface-craft. The thermal solver and the post-processing module are not discussed in this paper.

Within this paper we present results for the modules and preliminary results for a generic rover in a lunar environment. Besides we discuss the general outline and point out the next steps in the development of the TherMoS tool.

1. BACKGROUND

The surface of the Moon is a harsh thermal environment for surface vehicles (rovers) and astronauts. Global temperature extremes range between 400 K at a sub solar point on the lunar equator around lunar noon and 40 K and below in permanently shadowed craters at the lunar poles. On a local scale the temperature varies even more due to the unique thermal properties of the lunar regolith and the lack of an atmosphere. Moreover, craters, boulders, or mountain ranges can significantly alter local surface temperatures, which in turn have an impact on the accessibility and safety of regions of exploration interest, as well as on the performance of surface craft. The goal behind the work summarized in this paper is to answer the question in which cases and on which scales dynamic calculations of thermal problems are helpful for the thermal engineer, systems engineer or project manager of space missions, in contrast to the common minimum/maximum approach. The work is based on the Thermal Moon Simulator (TherMoS), a tool programmed in MATLAB®, which is specifically adapted to the demanding thermal conditions on the lunar surface. Its objective is to provide mission planners and surface craft designers the means of forecasting the thermal environment at points of interest in a given period during a lunar day.

2. STATE OF THE ART

Current surface-craft (rovers and spacesuits) planned for surface operations on the Moon (e.g. the European Mobile Payload (MPE) element on the European Space Agency (ESA) 'Lunar Lander' (LL)) are designed to worst case considerations which account for the hottest and coldest cases expected on the mission. The thermal control methods are thus designed to meet those static cases but are not necessarily suitable for transient effects occurring in the lunar surface environment. The thermal environment on the lunar surface has been subject to research for almost 80 years. Infrared measurements [1] as well as microwave measurements [2] led to a multitude of mathematical models of the lunar surface temperature, especially in the fifties and sixties of the 20th century [3-5]. With the beginning of space flight and the first probes sent to the Moon, new ways of measurement became available and new models of the temperature distribution on the Moon arose [6]. During the Apollo-Era new challenges emerged for scientists as well as engineers, who had to analyze whether humans and space-/surface craft were able to survive and function in the harsh lunar environment [7]. With the data obtained during Apollo, more sophisticated temperature models were feasible [8], showing for example that thermal anomalies could be localized in regions with boulder fields or differences in local bedrock [9,10]. Two decades later, as the question emerged whether ice could endure in craters on the Moon, new scientific models focused on the poles [11,12]. The renewed launch of space probes into orbits around the Moon (e.g. Clementine 1994, Lunar Prospector 1998, SMART-1, 2003) and the improvement in computer based modeling also created demand for new and more accurate thermal models [13,14]. Most of these models focus on the large scale temperatures of the lunar surface that alter slowly over one lunar day. Apart from the crater models [11,12] they do not account for local effects and none of them considers transient effects for moving surface-craft.

During the Apollo missions it became obvious that transient effects impact surface operations. The Apollo landings took place during lunar morning, in order to avoid the high temperatures of lunar noon[1]. Still the rubber wheels of the Modular Equipment Transporter (MET) used on Apollo 14 were designed to sustain minimal temperatures as low as 216 K. The temperature of one of the wheels dropped below that threshold only because it was shadowed by the other parts of the surface craft [15]. The impact of the thermal environment on equipment might have been addressed differently if more detailed thermal models of the lunar surface had been available.

The thermal environment is an up-to-date issue for scheduled rover missions to the Moon. High surface temperatures cause high heat loads on the undercarriage of rovers [16]. Boulder shadows provide a significant cold spot [17]. Optical systems (e.g. telescopes) have stringent requirements on thermal stability [18]. Power generating systems such as radioisotope thermoelectric generator (RTGs) or sterling radioisotope generators (SRGs), often used for probes and rovers in regions where the Sun cannot provide sufficient energy, form local heat sources on the surface-craft besides producing electrical energy [19]. The dimensioning and ability of thermal control systems to address high or fluctuating inner loads for a roving vehicle in combination with an altering environmental temperature profile makes dynamic thermal simulations for rovers highly attractive.

The thermal environment has also proven to be a major challenge in the design of extra-vehicular activity (EVA) suits. During the last 30 years of EVAs, several cases of thermal environment related discomfort were reported [20,21]. These reach from discomfort due to hypothermia in shadowed areas to the abort of an EVA caused by visor fogging related to thermal cycling [20]. The liquid cooling garment (LCG), a part of the suits' active thermal control (ATC) dedicated to transporting heat away from the body, is mainly controlled manually by the astronauts. During extravehicular activities the primary tasks require a lot of concentration. This can lead to lack of attention of the astronaut towards the adjustment of the EVA suit ATC. This in turn can lead to thermal imbalances [20].

Not to waste water by sublimating it is a requirement for future lunar surface EVA suits [22,23]. With that radiators become the primary way to shed excess heat. New concepts for radiators emerge as the return to the Moon is being considered. These concepts are for example digital radiators [24] and electrochromic radiators [22]. The use of radiators in turn demands a more detailed knowledge of the spacesuit geometry and thermal behavior as well as the local (lunar) environment [25,26]. Especially electrochromic radiators show promise in the thermal control of future space suits. But this technology demand fast control algorithms to optimize heat rejection in connection with the astronaut's posture, velocity and thermal environment. Here a static minimum/maximum analysis and dimensioning is not deemed sufficient.

Current thermal tools like Thermal Desktop®, ESATAN-TMS® or Thermica® are well suited to account for the thermal design questions arising in orbits around the Earth or other celestial bodies. When it comes to surface operations no functionality is currently implemented in ESATAN-TMS r4® as well as in Thermal Desktop® to the best of our knowledge. Simplified spherical bodies are assumed in Thermica® [27]. This lack of detailed models shall be overcome with the TherMoS simulation, of which the current status is presented in this paper.

3. THE THERMOS TOOL

The TherMoS tool has the goal of providing a simulation environment that enables calculations of temperatures in and on moving surface-craft on the lunar surface. It rests upon the hypothesis that a transient calculation of temperatures benefits thermal design of surface craft with low thermal inertia such as exploration rovers or surface-craft with high agility and narrow survival temperature ranges such as astronauts in spacesuits. By performing detailed case study simulations simplified rules of thumb shall be derived for the design and operation of moving surface craft on the lunar surface.

The TherMoS tool is implemented in MATLAB® with an extension in NVIDIA OptiX®. In its current status the TherMoS tool consists of several sub-modules which are a Global Topographic Module, a Regolith Layer Module, a Crater & Boulder Module, an Orbit Propagator & Lunar Orientation Module, a Ray Tracing Module and a Geometry Preprocessing Module. In addition, there are

[1] A synodic lunar day (called *lunation*) lasts 29,5 Earth days. Lunar morning or noon thus refers to a time frame of several Earth days.

the solver and post-processing modules, which will not be discussed in this paper.

3.1. The Global Topographic Module

The global topographic model for the TherMoS tool is based on a publicly available dataset measured by the LALT (Laser ALTimeter) instrument onboard the Japanese probe Kaguya. On a large scale and at the poles the topologic features are well represented due to a high density of data points. Features in the range of the spatial resolution of the instrument (1.8 km at the Moon equator) appear to have smoother slopes than in reality. Features with a size <1.8 km such as small craters, boulders, and steep cliffs (as well as the Hadley Rille) could not be measured by the LALT instrument [28]. This lack of information in the small feature range led to the implementation of the Crater & Boulder Module (see section 3.3).

The current implementation for the global topography in TherMoS allows to decide between flat square representation for small patches (<100 km), as well as convex circular elements for larger regions. Additional views are possible, such as a panoramic view from a certain spot. In the following figures the Apollo 15 landing site was chosen as example. In Figure 1 a rectangular patch is depicted with an edge length of 36 km. In Figure 2 a circular topographic map of the same region is shown. Here the diameter of the shown patch is 300 km. In Figure 3, a panorama of the same position is shown. The depth of the panorama is 25 km.

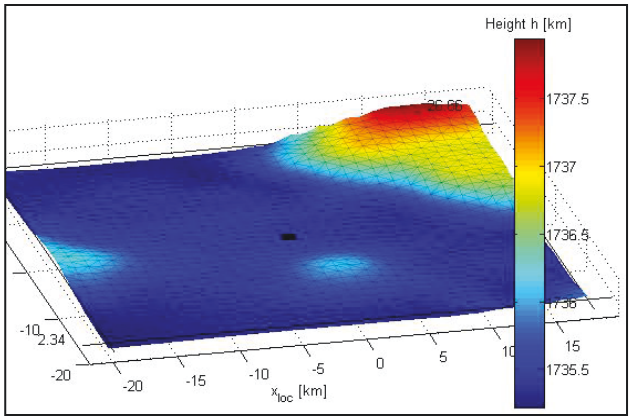

Figure 1: Topographic map of the Apollo 15 landing site, based on Kaguya data (36 km). Region with higher resolution in center

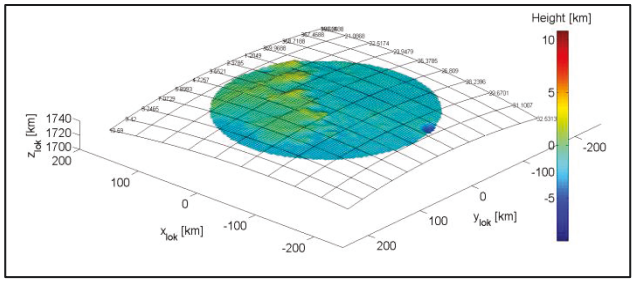

Figure 2: Topographic map of the Apollo 15 landing site, diameter 300 km.

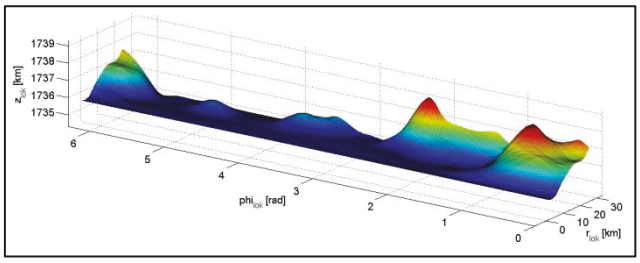

Figure 3: Unwrapped illustration of the panorama of the Apollo 15 landing site (maximum distance 25 km) r_{lok} is the distance from the center and phi_{lok} represents the circumference.

3.2. Regolith Layer Module

A central part of any thermal simulation for the lunar surface is a model of the lunar regolith with its unique thermal properties. A multitude of models for lunar regolith have been proposed in the past [1-8,11-14] as already discussed in section 2. Most of these models focus on a flat plane and average temperatures on the Moon. They agree in that the temperature variation on the Moon mainly depends on the thermal inertia γ [$J \cdot m^{-2} \cdot K^{-1} \cdot s^{-1/2}$] of the lunar regolith:

$$= (k \cdot \rho \cdot c)^{1/2} \quad (1)$$

where k is the thermal conductivity [$W \cdot m^{-2} \cdot K^{-1}$], ρ is the density [$kg \cdot m^{-3}$] and c is the specific heat [$J \cdot kg^{-1} \cdot K^{-1}$] of lunar regolith. The temperature also depends on the lunar infrared emissivity ε [-], its solar absorptivity α [-], the albedo A [-] or reflectivity respectively, the solar constant S [$W \cdot m^{-2}$] [15] and its angle of incidents β [°].

The large number of models was reviewed and clustered into three classes (two layer models, particulate models and finite element models). Of each class one model was rebuilt in MATLAB®.

In the first class of models the conductivity and the specific heat of the regolith vary with temperature, the density is regarded as being constant. The surface is considered to be made of two layers. The upper layer with only several millimeters of thickness was considered to be made of finer material. The layer underneath modeled of coarser but denser material. One of these models was presented by Cremers et al. [8, 29]. It did not account for the internal heat flux, different regolith densities and used a solar heat flux that was too low. The purpose of that model was to analyze the properties of samples from the Apollo missions.

An alternative approach are particulate models to compute the lunar surface temperature [4,6]. Winter et al. [6] proposed to simulate the grainy consistency of the lunar regolith as an array of cubes in several layers. The cubes were only connected through the connecting corners, resulting in a radiation dominated heat transfer through the regolith.

The third class of models examine the temperature distribution on a local scale [11,12]. In the topographic thermal model published by Salvail and Fanale [12] a crater was divided into finite elements. Each element received direct solar radiation, reflected radiation from other crater elements and emitted radiation into its environment.

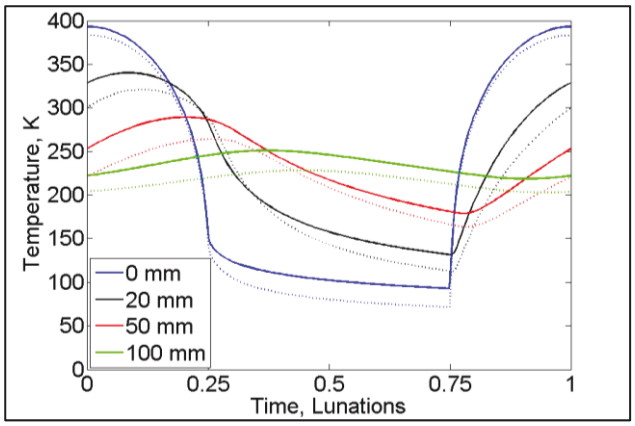

Figure 4: Comparison of lunar equatorial temperatures according to Cremers (full line) [8, 29] and Winter [6] (dashed line) relative to one lunar day (= lunation = L). The depth within the regolith layer is given in millimeter.

In Figure 4, the results of the reproduced MATLAB models of Cremers et al. (full lines) and Winter et al. (dashed lines) are compared.

The TherMoS regolith layer model is based on the work performed in Cremers et al. [8]. In contrast to Cremers et al., a depth dependent regolith density and a heat flux from the interior of the Moon was implemented [30]. Figure 5 shows the density distribution for the interval of 0 m to 2 m of depth for slope angles of 0° (full line) and 15° (dashed line). The regolith layer consists of an arbitrary number of heat nodes between 0 and 2 m of depth. For each layer the density, heat capacity, thermal conductivity, and the connecting interfaces are calculated.

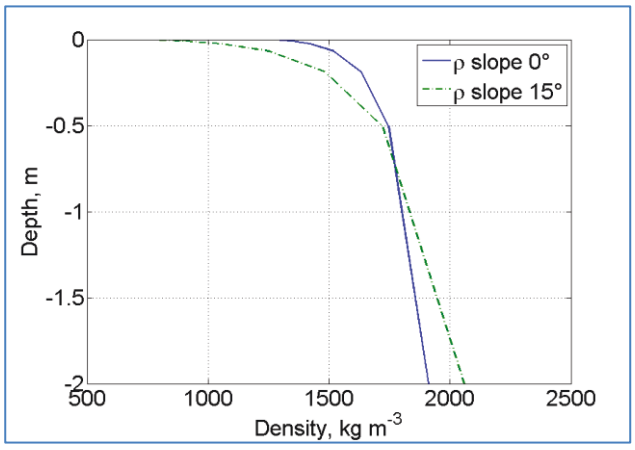

Figure 5: Density distribution between 0 and 2 m depth for slope angles of 0° and 15°.

To calculate the temperature of each depth node, incoming and outgoing heat fluxes are computed. These heat fluxes depend on local latitude and time of lunar day as well as on the surface element temperature of the precursory time step. In Figure 6, the temperature development is shown for a case with 10 depth nodes at the lunar equator.

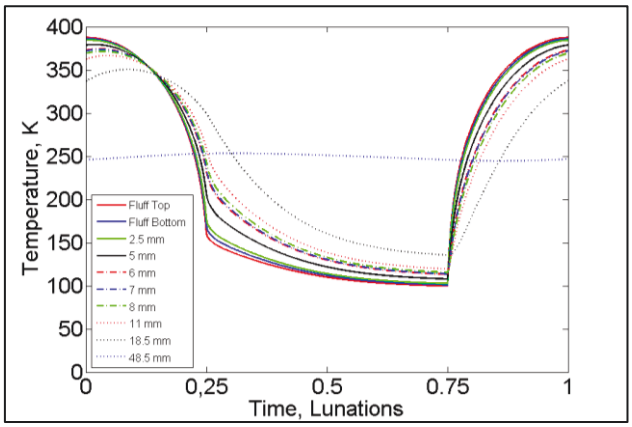

Figure 6: Temperature computed with the TherMoS regolith layer model for a 1 m² face at the lunar equator for one lunar day at different depth.

3.3. Crater and Boulder Module

The lunar surface is covered with a multitude of craters created by impacting bodies. The crater profile varies from simple bowl shaped craters to complex craters with flat floors and central peaks or ring structures [31]. The crater ejecta which are excavated during the cratering process can form secondary craters around the primary ones [31,32]. For the TherMoS crater model only small primary craters with a diameter up to 20 km are considered. Larger ones are part of the topographic map.

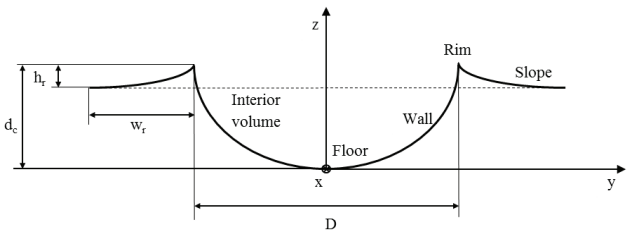

Figure 7: Simple crater schematic with local coordinate system [31,33].

The small crater morphology and nomenclature is described in Figure 7 and can be calculated with the following equations [31]:

$$d_c = 0.196 \cdot D^{1.01} \quad (2)$$

$$h_r = 0.036 \cdot D^{1.014} \quad (3)$$

$$w_r = 0.257 \cdot D^{1.011} \quad (4)$$

They include the crater diameter D [km], the crater depth d_c [km], the rim height h_r [km] and the rim width or slope length w_r [km]. The parabolic shape of the crater wall and the crater slope [34] is given by the respective z-coordinate in the crater coordinate system (see [31]):

$$z_{wall} = 0.784 \cdot D^{-0.99} \cdot y^2 \quad (5)$$

$$z_{slope} = -0.545 \cdot D^{-1.08} \cdot y^2 \quad (6)$$

The relative crater frequency per area - the crater density - depends on the age of the lunar region [35]. The ancient highlands on the Moon have a high crater density of $1758 \cdot 10^{-4}$ [km^{-2}] of craters with diameter > 1 km (arithmetic

average) [35]. The lunar mare regions are younger and thus show a smaller crater density that ranges from only $30 \cdot 10^{-4}$ to $90 \cdot 10^{-4}$ [km^{-2}] for craters with a diameter of > 1 km [35].

Due to the excavation and ejection process during the crater formation, 5% of the crater mass disperses around the crater as boulders [36]. The remaining material forms a granular material. The maximum boulder diameter B_{max} [km] depends on crater size and is given by [32,36]:

$$B_{max} = 0.1 \cdot K \cdot D^{2/3} \quad (7)$$

Based on the different impact velocities, the correlation factor K and therefore the boulder size varies for primary (K = 0.29, used for this boulder model) and secondary craters (K = 0.46) [32]. The bedrock material has no influence on the maximum boulder size B_{max} [32, 38], but on boulder distribution around the lunar mare and highland craters. In highland regions 65% of the boulders lie within the crater. In the mare regions only 10% lie inside the crater rim [38]. In both cases most of the boulders are within an area up to 2 crater radii away from the crater center [38]. Boulders penetrate approximately to a depth of 31% of their diameter into the regolith [39]. The current TherMoS boulder and crater model does not account for boulders inside craters, the penetration depth and the coverage with lunar regolith is neglected.

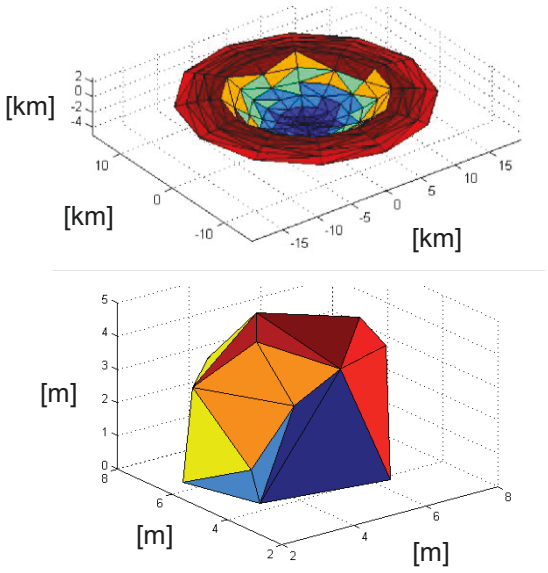

Figure 8: Model for a lunar crater and an arbitrary boulder of 4 m diameter.

Based on these equations and assumptions the TherMoS Crater and Boulder model creates arbitrary landscapes. These landscapes are then combined with the global topographic landscape discussed in section 3.1. Figure 8 shows a primary crater and an arbitrary shaped boulder as created by the TherMoS Crater & Boulder Model. Figure 9 shows the random arrangement of craters in the diameter range of $D \leq 20$ km on a section of 100×100 km^2 taking crater overlapping into consideration. Boulders are distributed outside the crater up to a distance of 2 crater radii (see Figure 10). The boulder size varies up to B_{max} and the bulk volume equates to 5% of the calculated interior crater volume.

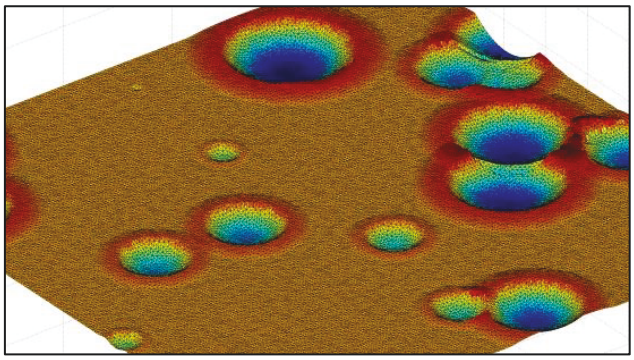

Figure 9: Lunar surface 100 x 100 km² with overlapping craters of diameters < 20km.

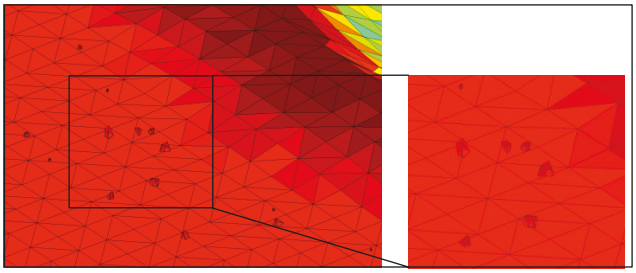

Figure 10: Boulder distribution around a crater.

3.4. Orbit Propagator & Lunar Orientation Module

In order to calculate the local temperatures it is crucial to determine the incoming heat fluxes. Thus it is important to predict azimuth and elevation of the Sun throughout a lunar day. The observer's position on the lunar surface as well as the local slope has to be taken into account. With regard to launch windows and missions in the future, the celestial dates have to be integrated. Therefore it was necessary to implement a combination of an orbit propagator and the possibility to determine the orientation of the Moon in space.

The lunar orbit is quite asymmetric and so its orbital parameters – inclination, semi-major axis, eccentricity, argument of perigee, and right ascension of the ascending node – are not at all constant but are subject to a number of perturbations. Particularly the Sun's gravitational influence, which is slightly more than twice the Earth's gravitational influence, is responsible for these effects [40]. Thus, perturbing acceleration acting on the Moon directed towards the Sun at all times. As the Moon is in synchronous rotation with Earth, it nearly always keeps the same side faced towards the Earth, but because of the optical and physical libration approximately 59% of the lunar surface can be observed from Earth. The model implemented in TherMoS is based on the VSOP2000A [41] planetary model which is used to calculate the heliocentric position of the Earth's center and the geocentric position of the lunar center at any given time. This model is complemented by the calculation of the optical libration angle [42] and an algorithm to determine the visibility of the Sun in percent.

Some simplifications were made in the TherMoS tool. The physical libration is neglected due to the very small amplitude [43] and the Moon is approximated by a sphere with a constant radius and not modeled as the ellipsoid it truly is.

The orbit propagation and lunar orientation simulation calculates the azimuth and elevation of the Sun's center its topmost and lowermost point, the percentage of the visible solar disc, and the azimuth and elevation of the Earth's center.

The calculation of the position of the Moon with respect to the Sun produced a maximum error of 47.24 km total compared to data calculated with online tools from the Jet Propulsion Laboratory (JPL) and the Institut de Méchanique Céleste et de Calcul des Éphemerides (IMCCE).

The azimuth and elevation results were compared to data obtained with the Satellite Tool Kit 9® (STK). The differences between the calculated and the STK data are smaller than 1.06° in azimuth and 0.46° in elevation. Figure 11 shows the deviations in the angle of incidence of the solar rays. During the course of the year 2011 the maximum deviation is about 1.15°. Figure 12 shows exemplary Sun azimuth and elevation for an observer at the Apollo 15 landing site throughout January 2012.

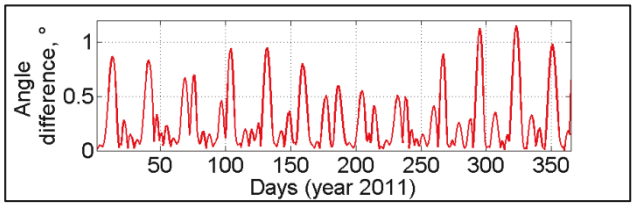

Figure 11: Deviations between the TherMoS orbit propagation and lunar orientation model from values calculated by STK for the Apollo 15 landing site.

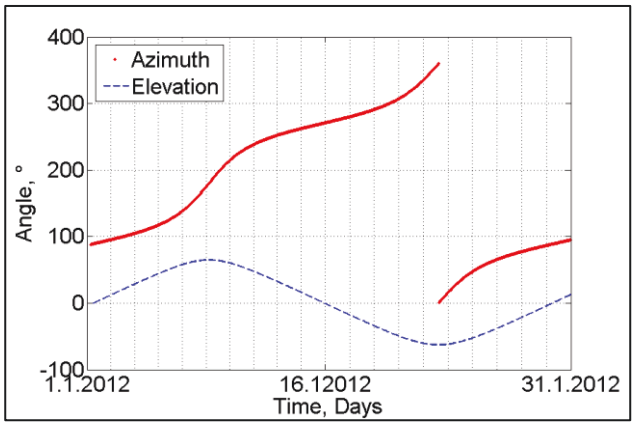

Figure 12: Azimuth and Elevation of the Sun's disc center at the Apollo 15 landing site for January 2012.

3.5. Ray Tracing Module

In order to calculate the heat transferred by radiation between different surface elements in the TherMoS simulation it is not enough to calculate only the *incoming* heat flux from the Sun. This heat *exchange* between surface elements is especially important for local surface features such as boulders and craters as well as for surface-craft placed within a lunar scene. Simple view factor determination is not enough if the surface craft is supposed to be moving. Ray tracing allows the determination of the heat that is exchanged by approximating the radiated energy bundles as discrete rays. The TherMoS Ray Tracing Module is implemented in the NVIDIA OptiX® framework, which provides the background for ray tracing computations on the graphics processing unit (GPU).

In the forward ray tracing approach used for TherMoS, the rays are generated in the radiation sources and propagated through a 3D scene. By determining and processing all intersections of these rays with scene objects it is possible to estimate the incoming and outgoing heat fluxes for each surface element. The implemented algorithm distinguishes between direct Sun rays, carrying the most part of the energy, and the infrared (IR) rays, radiated by all surfaces depending on their temperature.

Figure 13 shows the interaction between MATLAB® and NVIDIA OptiX®. Initialized from the MATLAB® script, the 3D models of the Moon scene and a surface craft are discretized in OptiX® as triangle meshes. The meshes are represented as sets of triangular faces and vertices. Assigned to each surface face are optical material properties such as reflectivity, emissivity and absorptivity. In addition, MATLAB® provides a temperature for each surface face.

The Ray Tracing Module computes the heat fluxes of the emitted/absorbed radiation for all geometry faces by accumulating the heat of the incoming rays and subtracting the heat fluxes of the emitted infrared radiation.

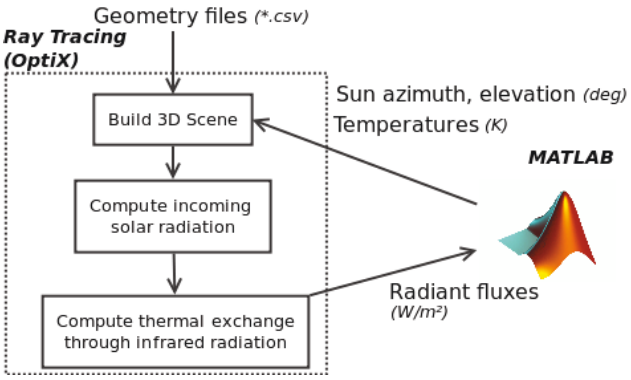

Figure 13: Processes, calculations and interaction performed in and between NVIDIA OptiX® and MATLAB®.

It is assumed that all solar rays are parallel and carry equal heat loads. A fixed value of 1376 [W·m^{-2}] for the solar heat flux was used. IR rays are sampled randomly over a unit hemisphere in a cosine-weighted fashion [44]. The emitted power carried by infrared rays is computed for every face of the mesh using the Stefan-Boltzmann law:

$$= \varepsilon \cdot \sigma \cdot A \cdot T^4 \qquad (8)$$

with ε being the emissivity [-], A the surface's area [m²], T the surface's temperature [K] and σ the Stefan-Boltzmann constant equal to 5.670373·10^{-8} [W·m^{-2}·K^4].

The objects are considered to have Lambertian surfaces, as they reflect equally and uniformly in all directions. Every ray hitting the surface is partly absorbed and partly reflected diffusely in random directions. The incident point of a ray serves as the origin for reflected rays. This process continues until the incoming ray has either reached its maximum number of reflections or is directed towards space. Depending on the surface that is hit, the

power carried by a ray diminishes until a certain threshold is reached and the ray progression is terminated by the algorithm. In the current simulation, a solar albedo of 0.12 is used for all Moon surface faces as suggested in [13]. The IR emissivity of the Moon surface is set to 0.97 as a fixed value for the temperature range from 102 K to 384 K [13].

The implemented Ray Tracing Module was tested on several geometries, including different refinements of an Apollo 15 landing site scene as well as artificial geometries with craters and boulders. The time needed for processing solar rays is mostly independent of the geometry size, and increases with the number of rays. The maximum test time of 1.32 seconds was reached for 20.000 faces in the Apollo 15 scene for solar rays. In the same scene it took 5.5 seconds to compute the IR rays with 500 rays per face. Figure 14 shows the result of a ray tracing performed on a random crater scene with 16.200 surface elements and a Sun elevation of 60°. This image was rendered in OptiX®.

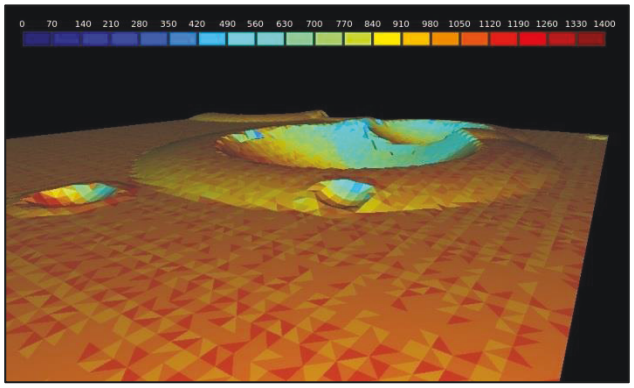

Figure 14: Heat fluxes [W·m^{-2}] for a random crater scene with 16.200 surface elements at a Sun elevation angle of 60°.

3.6. Geometry Preprocessing Module

Thermal analysis of structures in the lunar environment requires detailed knowledge of geometrical as well as physical properties. The Geometric Preprocessing Module of the TherMoS tool serves in obtaining these properties and associating them for a combined output. An object oriented approach was chosen in contrast to procedural programming, because it focuses on data itself. Information and functions are encapsulated into one object, while its structure can be inherited for code reusability [45].

In order to form links between structural data and material characteristics, the model is split into several segments, their number determined by resolution requirements and computer performance [46]. Each segment is assigned a set of properties and is subsequently indexed by a unique identity (ID). When the whole model is defined it can be forwarded to the solver. Once processed, the thermal behavior of each element can be displayed.

The Geometric Preprocessing Module is an intricate part of the TherMoS environment. While input data is generally not restricted to any format [47], the combined output needs to adhere to a certain structure, depending on solver and Ray Tracing Module prerequisites. In TherMoS, a matrix with the necessary data is forwarded to the Ray Tracing Module as well as to the solver. Figure 15 shows the basic architecture of the Geometry Preprocessing module with the combined matrix as main output.

As a result of the interactive nature of model assembly and property allocation, a GUI (Graphical User Interface), shown in Figure 16, has been selected as method of choice. The GUI consists of a tabbed structure that comprises one tab for each of the three main tasks: Import, Assembly, and Export.

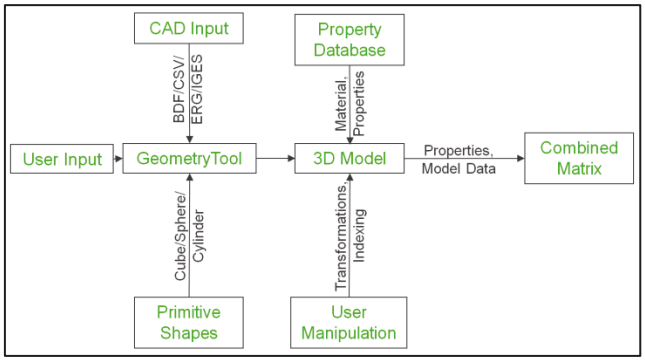

Figure 15: TherMoS Geometry Preprocessing Module Architecture.

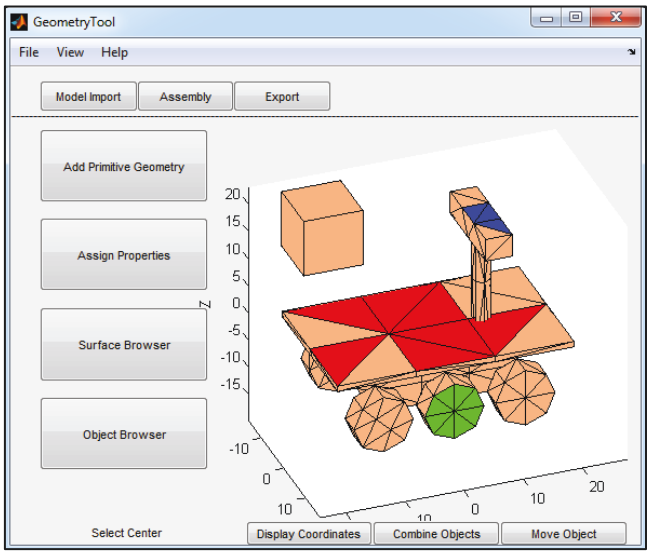

Figure 16: Geometric Preprocessing Module: The User Interface shows the basic layout of the TherMoS Geometry Preprocessing Module with in-and outputs for a generic rover.

Initially, relevant model data is extracted from external sources. Currently supported data types are BDF (from Nastran), IGES (from CATIA), ERG (from ESARAD) as well as CSV. Segmentation is achieved by converting 3D shapes to a cluster of nodes and a collection of triangulated surfaces [48]. The former represents each grid point as it is registered in the x-y-z-coordinate system, while the latter procures a combination of three vertices to form a plane. Triangulation may also be applied as mesh simplification by reducing the amount of faces while maintaining the general shape [49]. Each surface element of an object represents an individual data point and possesses a unique number for indexing. If more than one object is present, the newest will yield to the numeration of the previous, i.e. surface-counting continues progressively.

The assembly tab provides functions for adding additional primitive shapes (cubes, spheres, cylinders). Surfaces for property allocations are selected interactively from the plot itself. Material data is imported from a modifiable Microsoft Excel® database [50]. Batches of surfaces can be combined in groups, if they share identical properties. Geometrical and corresponding physical information is automatically saved within object oriented MATLAB®-structs.

Export functionality to diverse formats exists for CSV, ERG, and an assortment of preliminary MATLAB compositions.

4. DISCUSSION

In the field of modeling and simulation, assumptions and simplifications are inevitable. In this chapter we discuss their impact on the status of the TherMoS tool.

The use of Kaguya data for the implementation of the topographic map has the disadvantage that it cannot be compared directly with data obtained by the Lunar Reconnaissance Orbiter (LRO). The coordinate frames that were used for the data sets of the two probes differ slightly. In order to compare temperatures calculated with the TherMoS tool, based on Kaguya topographic data, with temperature data measured with LRO Diviner data, it will be necessary to either perform a suitable coordinate transformation or to rely entirely on LRO data.

The current Regolith Layer Module of TherMoS uses material properties and heat fluxes that were measured during the Apollo era either *in-situ* or in samples returned to Earth. The extrapolation of these material properties to the entire Moon leads to errors. The thermal as well as the optical properties of regolith differ from region to region. This is due to a large variety in geological composition of the regolith. It is not part of this work to address these differences. In the future, existing geological maps of the Moon might be included in the TherMoS tool. In order to gain the most accurate temperature calculation it will be inevitable to use detailed information of the region of interest.

With the boulder and crater model local lunar scenes can be created randomly. The craters are created based on a predefined shape and not formed due to simulated events. Thus there is no overlay of older craters with ejecta material from younger craters. The overlay of different craters is idealized, which leads to the effect that crater rims are always sharp edges and not degraded. Ejecta layers and rim edges impact the temperature calculations. For the current stage it is not sensible to detail the craters any further. If a landing site is determined one could build a refined model based on images taken with high resolution cameras from orbit.

The module does not yet account for boulders inside craters. This is an ongoing process and will be implemented in the near future. For craters in the mare regions this is of no big concern but for highland regions, interesting for currently proposed lunar missions, those boulders are important. The boulder coverage with regolith is currently not accounted for, which might lead to an additional error in boulder core temperature. It needs to be determined how large the insulating effects of layers of regolith are.

The forward ray tracing provides an easy way to compute reflections and diffuse radiation, because the algorithm simulates the natural distribution of the radiation. A disadvantage of this approach however is the high number of rays that do not hit any objects. An alternative to the forward ray tracing approach is backward ray tracing, where the rays are generated from the objects to the light sources, in order to estimate how much radiation reaches the surface. Since in the backward ray tracing approach fewer rays have therefore to be generated it is more effective in terms of computation time demand. On the other hand, the simulation of reflections becomes more complicated. Backward ray tracing is also poorly suitable for simulating the infrared radiation, because the number of radiation sources in this case is equal to the number of faces.

The factor with the highest impact on performance in the forward ray tracing algorithm is the number of processed rays. The majority of emitted IR rays does not reach any objects but vanishes in space. An improved statistical approach could minimize the number of emitted IR rays. This approach with non-uniformly sampled IR rays would lead to a more complicated computation of the per-ray-energy. Another way to reduce the amount of generated IR rays would be to differentiate between a small area in the center of the scene with a high ray density and a less important area at the outer rim of the scene with fewer emitted IR rays per face. Both approaches need further study and one of those will be implemented eventually.

5. CONCLUSIONS & FUTURE WORK

The current status of the TherMoS tool developed at the Institute of Astronautics at the Technische Universität München was presented in this paper. The tool is able to create topographic maps based on Kaguya LALT measurements. The topography can be displayed in several ways to allow for large scale spherical maps, local square maps for temperature calculations as well as panorama views to get an impression of the local horizon for a surface-craft. The Regolith Layer Module relies on older models for lunar temperature calculations which use temperature dependent regolith thermal properties (thermal conductivity and heat capacity). The models were enhanced with a density dependency to allow for different slope angles. The model accounts for a regolith depth of about 2 meters and incorporates the lunar heat flow originating from the lunar interior. In this way the temperature of a given surface element can be calculated depending on time of lunar day (incident heat flux), temperature, internal heat flow, and slope angle.

The implemented orbit Propagator & Lunar Orientation Module relies on the VSOP2000A power series development approach. It is well suited to meet the needs of the current TherMoS simulation approach. It allows predicting the azimuth and elevation for an operator on the lunar surface for a user defined period.

The Boulder & Crater Module is able to represent a small section of the lunar surface with small simple craters not covered by topographic data obtained by remote sensing laser instruments. The module uses scientific data for the crater density, depending on the location being a mare or a highland region. Moreover, a boulder size distribution and boulder occurrence is implemented that depends on crater size. Thereby the Crater & Boulder Module

amplifies the resolution of the Global Topographic Module to form a more detailed lunar landscape.

The Geometry Module allows for the combination of geometries, such as the topography and artificial objects (spheres, cubes) or detailed surface craft. The Geometry Preprocessing Module moreover is capable of loading geometry files from different formats (IGES, BDF, ERG) and outputting them to ERG, CSV, or MATLAB® file formats. The Geometry Preprocessing Module provides the user with a graphical user interface that allows manipulating the geometries, to add materials and to associate these materials to surface elements or groups of surface elements. The Geometry Preprocessing Module also allows selecting surfaces inside the 3D plot. It can however be a tedious task, if the geometric object contains many elements.

In the future, the different modules will be further enhanced in order to allow the calculation of the temperatures for surface-craft and for the lunar surface. Thus a differentiation between mare and highland regolith will be implemented. The thermal inertia of boulders for thermal calculations will be addressed and further refined. The partial coverage of boulders with regolith and its effect on boulder core temperature will be addressed. With regard to future missions in lunar highland regions the possibility of placing boulders inside craters will be added. The computation time for the forward ray tracing algorithm is still high, caused by IR rays being emitted from every surface element. The forward ray tracing algorithm needs to be refined further in order to reduce computation time. The Geometric Preprocessing Module will be enhanced by a module to translate or rotate an object in a given period of time.

Long term goals of the entire endeavor are the comparison of results of a topographic map with values measured by LRO instruments (DIVINER data) to add surface craft geometries such as rovers and astronauts in spacesuits, and to add movements of surface-craft through scenes with boulders and craters. Ultimately, rule of thumbs will be derived for the thermal design of surface craft on the lunar surface.

6. ACRONYMS & ABBREVIATIONS

ATC – Active thermal control

BDF – Bulk data file (NASTRAN)

CSV – Comma separated values

ESA – European Space Agency

EVA – Extra vehicular activity

GPU – Graphics processing unit

GUI – Graphical user interface

IGES – Initial graphics exchange specification

IMCCE – Institut de Méchanique Céleste et de Calcul des Éphemerides

IR – Infrared

JPL – Jet Propulsion Laboratory

LALT – Laser Altimeter

LCG – Liquid cooling garment

LL – Lunar Lander

LRO – Lunar Reconnaissance Orbiter

LRT – Lehrstuhl für Raumfahrttechnik

MPE – Mobile Payload Element

RTG – Radioisotope thermoelectric generator

SRG – Stirling radioisotope generators

STEP – Standard for the exchange of product model data

STK – Satellite tool kit

TherMoS – Thermal Moon simulator

TUM – Technische Universität München

VSOP2000A - Variations Séculaires des Orbites Planétaires (2000 is the year of publishing)

7. ACKNOWLEDGEMENTS

The authors would like to acknowledge Martin Karanikolov for his work on the Regolith Layer Module, Frank Yannick Vogel and Alexander Lechner for their work with the Kaguya data to derive the global topographic map.

8. REFERENCES

[1] Pettit, E., Nicholson, S. B., "Lunar radiation and temperatures," *American Astronomic Society*, 71 – 102, 1930.

[2] Wesselink, A.J., "Heat conductivity and nature of the lunar surface material," *Bulletin of the astronomical institutes of the Netherlands*, Vol. 10, Issue 390, 1948, pp. 351 – 363.

[3] Jaeger, J.C., "The surface temperature of the moon," *Australian Journal of Physics*, Vol. 6, 10-21, 1953.

[4] Linsky, J.L., "Models of the Lunar Surface Including Temperature-Dependent Thermal Properties," *Icarus*, Vol. 5, 1966, pp. 606 – 634.

[5] Krotikov, V.D., Shuko, O.D., "The heat balance of the lunar surface layer during a lunation," *Soviet Astronomy Journal*, Vol. 7, No. 2, 1963, pp. 228-232, provided by the NASA Astrophysics Data System.

[6] Winter, D. F., Saar, J. M., "A particulate thermophysical model of the lunar soil," *The Astrophysical Journal*, Vol. 156, 1969, pp. 1135-1151.

[7] Menzel, D.H., "Temperature distribution of the Moon," *Philosophical Transactions of the Royal Society of London*, Series A, Mathematical and Physical Sciences, Vol. 264, No. 1150, A Discussion on Infrared Astronomy, 1969, pp. 141-144.

[8] Cremers, C. J.; Birkebak, R. C.; White, J. E., "Lunar surface temperatures from Apollo 12," *Earth, Moon, and Planets*, Vol. 3, Issue 3, 1971, pp. 346-351.

[9] Allen, D. A., "Infrared Studies of the lunar terrain - part I The background moon," *Earth, Moon, and Planets*, Volume 2, Issue 3, 1971, pp. 320–337.

[10] Allen, D. A., "Infrared studies of the Lunar terrain - part II thermal anomalies," *Earth, Moon, and Planets*, Volume 2, Issue 4, 1971, 435–462.

[11] Vasavada, Ashwin R.; Paige, David A.; Wood, Stephen E., "Near-Surface Temperatures on Mercury and the Moon and the Stability of Polar Ice Deposits," *Icarus*, Vol. 141, Issue 2, 1999, pp. 179-193.

[12] Salvail, J.R., Fanale, F. P., "Near-surface ice on Mercury and the Moon: A topographic thermal model," *Icarus*, Vol. 111, 1994, pp. 441-455.

[13] Racca, G. D., "Moon surface thermal characteristics for moon orbiting spacecraft thermal analysis," *Planetary and Space Science*, Vol. 43, Issue 6, 1995, pp.835-842.

[14] Christie, Robert J.; Plachta, David W.; Hasan, Mohammad M., "Transient Thermal Model and Analysis of the Lunar

Surface and Regolith for Cryogenic Fluid Storage," NASA TM-215300, 2008.

[15] Clawson, J.F., Tsuyuki, G.T., Anderson, B.J., Justus, C.G., Batts, W., Ferguson, D. and Gilmore, D.G., "Spacecraft Thermal Environments," *Spacecraft Thermal Control Handbook* / edited by David G. Gilmore, Volume 1: Fundamental Technologies, 2nd edition, 2002, pp. 21 – 69.

[16] Gump D.A., Thornton J., "Prospects for Robotic Lunar Exploration by Commercial Enterprise," *Proceedings of the 32nd IEEE Aerospace Conference*, IEEEAC paper #1463, 2011.

[17] Barraglough S., Huston K., Allouis E., "Thermal Design for Moon-NEXT Polar Rover," *Proceedings of the 39th International Conference on Environmental Systems*, SAE Paper 2009-01-2461, 2009.

[18] Pecson J., Boyd D. A., Hashemi A., Aaron K., Ambrose J., Maddox J. F., Mattison E. M., Vessot R. F. C., "Precision Temperature Control," *Spacecraft Thermal Control Handbook* / edited by David G. Gilmore, Volume 1: Fundamental Technologies, 2nd edition, 2002, pp.739 – 666.

[19] Shaltens, R. K., "Future Opportunities for Dynamic Power Systems for NASA Missions," International Stirling Forum, 2006.

[20] Katuntsev, V. P.; Osipov, Yu. Yu.; Barer, A. S.; Gnoevay, N. K.; Tarasenkov, G. G., "The main results of EVA medical support on the Mir Space Station", *Acta Astronautica*, Vol. 54, Issue 8, 2004, pp.577–583.

[21] Barer, A. S., "EVA medical problems", *Acta Astronautica*, Volume 23, 1991, pp.187–193.

[22] Metts, J. G.; Klaus, D. M. (2009), "Conceptual Analysis of Electrochromic Radiators for Space Suits," *Proceedings of the 39th International Conference on Environmental Systems,* SAE Paper 2009-01-2570, 2009.

[23] Fullerton, R. K., "Advanced EVA Roadmaps and Requirements," *Proceedings of the 31st International Conference on Environmental Systems*, SAE Paper 2001-01-2200, 2001.

[24] Ganapathi, G. B.; Sunada, E. T.; Birur, G. C.; Miller, J. R.; Stephan, R, "Design Description and Initial Characterization Testing of an Active Heat Rejection Radiator with Digital Turn-Down Capability", Proceedings of the 39th International Conference on Environmental Systems, SAE International, 2009-01-2419, 2009.

[25] Ochoa, D. A.; Miranda, B. M.; Conger, B. C.; Trevino, L. A.," Lunar EVA Thermal Environment Challenges," *Proceedings of the 36th International Conference on Environmental Systems*, SAE Paper 2006-01-2231, 2006.

[26] Ochoa, D. A.; Vogel, M. R.; Trevino, L. A.; Stephan, R. A., "Potential of a New Lunar Surface Radiator Concept for Hot Lunar Thermal Environments," *Proceedings of the 38th International Conference on Environmental Systems*, SAE Paper 2008-01-1960, 2008.

[27] Soriano, T. "Lunar Base Thermal Analysis with THERMICA," *prepared for the 40th International conference of Environmental Systems, Barcelona, 2010, not published – personal communication*, 2011.

[28] Araki, H.; Tazawa, S.; Noda, H.; Ishihara, Y.; Goossens, S.; Sasaki, S.; Nawano, N.; Kamiya, I.; Otake, H.; Oberst, J.; Shum, C., "Lunar Global Shape and Polar Topography Derived from Kaguya-LALT Laser Altimetry", *Science*, Volume 323, Issue 5916, 2009, pp. 897–900.

[29] Cremers CJ, Birkebak RC, White JE: "Lunar Surface Temperatures at Tranquility Base", *AIAA Journal*, vol. 9 No. 10, p.1899-1903.

[30] Hager, P., Karanikolov, M., Lechner, A., Vogel, Y., „A lunar surface environment model for the thermal moon simulator", *Proceedings of the 41st conference on environmental systems AIAA*, Portland, USA, 2011.

[31] Hörz, F., Grieve, R., Heiken, G., Spudis, P., and Binder, A., "Lunar Surface Processes", in *The Lunar Sourcebook – A user's guide to the Moon*, Cambridge University Press, New York, Port Chester, Melbourne, Sydney, 1991, pp. 61-120.

[32] Bart, G. D., Melosh, H. J., "Using lunar boulders to distinguish primary from distant secondary impact craters", *Geophysical Research Letters*, Vol. 34, L07203, doi:10.1029/2007GL029306, 2007.

[33] Mitchell, J. K, Houston, W. N., Scott, R. F., Costes, N. C., Carrier, W. D. III, and Bromwell, L. G., "Mechanical properties of lunar soil: Density, porosity, cohesion, and angle of internal friction", *Proceedings of the Lunar Science Conference (3)*, 1972, pp. 3235–3253.

[34] Turtle, E. P., Pierazzo, E., Collins, G. S., Osinski, G. R., Melosh, H. J., Morgan, J. V., and Reimold, W. U., "Impact structures: What does crater diameter mean?", *in* Kenkmann, T., Hörz, F., and Deutsch, A., eds., *Large meteorite impacts III*: Geological Society of America Special Paper 384, 2005, pp. 1–24.

[35] Neukum, G., and Ivanov, B. A., "Crater Size Distributions and Impact Probabilities on Earth from Lunar, Terrestrial-planet, and Asteroid Cratering Data", *in* T. Gehrels (ed.), *Hazards due to Comets and Asteroids*, Univ. of Arizona Press, Tucson and London, 1994, pp. 359–416.

[36] Cintala, M. J., Garvin, J. B., and Wetzel, S. J., "The distribution of blocks around a fresh lunar mare crater", *Lunar and Planetary Science XIII*, 1981, pp. 100-101. Abstract.

[37] Moore, H. J., "Large blocks around lunar craters", *Analysis of Apollo 10 Photography and Visual Observations*, NASA SP-232, 1971, pp. 26.

[38] Lee, S. W., Thomas, P., and Veverka, J., "Phobos, Deimos, and the Moon: size and distribution of crater ejecta blocks", *Icarus*, Vol. 68, Issue 1, 1986. pp. 77–86.

[39] Hovland, H. J., and Mitchell, J. K., "Boulder tracks and nature of lunar soil", *The Moon*, Vol. 6, Issue 1-2, 1972, pp. 164–175.

[40] Weigert,A., Wendker, H. J., Wisotzki, L., "Astronomie und Astrophysik" Potsdam: WILEY-VCH, 2009, p. 110

[41] Moisson, X., Bretagnon, P., "Analytical Planetary Solution VSOP2000", *Celestial Mechanics and Dynamical Astronomy*, 80, 2001, pp. 205-213.

[42] Taylor, D. B., Bell, S. A., Hilton, J. L., Sinclair, A. T., "Computation of the Quantities Describing the Lunar Libration in The Astronomical Almanac", *NAO Technical Note*, 74, 2010

[43] Unsöld, A., Baschek, B., "Der Neue Kosmos Einführung in die Astronomie und Astrophysik", Heidelberg: *Springer,* 2005, p. 19.

[44] Dutre P., „Global Illumination Compendium", p.19, 2003

[45] Svenk, G., "Object-Oriented Programming: Using C++ for Engineering and Technology", *Delmar*, 2002, pp.107–109.

[46] King, J., "Matlab 6 for Engineers: Hands-On Tutorial", *R T Edwards Inc*., 2001, pp.157–158.

[47] Wohlfarth, U.; Rau, M.; Beuschel, M.; Angermann, A., "MATLAB - Simulink - Stateflow: Grundlagen, Toolboxen, Beispiele", Oldenbourg Wissenschaftsverlag, 2011, pp.38–41.

[48] Roderer, H., "Grafik in MATLAB: Ein Kompendium", *GRIN*, 2011, pp.61–62.

[49] Olling, G.J.; Choi, B.K.; Jerard, R.B., "Machining Impossible Shapes", Vol. 18, *Springer US*, 1999, pp.173–174.

[50] Moaveni, S., "Engineering Fundamentals: An Introduction to Engineering", Wadsworth Inc. Fulfillment, 2011, pp.487–489.